

# A Study on the Intralaminar Damage and Interlaminar Delamination of Carbon Fiber Composite Laminates Under Three-Point Bending Using Acoustic Emission

P. F. Liu · J. Yang · B. Wang · Z. F. Zhou ·  
J. Y. Zheng

Submitted: 30 July 2014/in revised form: 19 October 2014/Published online: 11 November 2014  
© ASM International 2014

**Abstract** The complicated failure mechanisms are always distinct features of composite materials which largely affect the stiffness and strength as well as the structural integrity. Yet, until now there are still no mature methods based on various test approaches for accurately predicting the failure mechanisms and damage evolution behaviors of composite structures by considering the effects of loads, environments, and material defects. This research designs and prepares the  $[0^\circ_{16}/0^\circ_{16}]$ ,  $[30^\circ_{16}/30^\circ_{16}]$ , and  $[15^\circ/-15^\circ]_{3s}/[15^\circ/-15^\circ]_{3s}$  carbon fiber composite specimens with initial interlaminar cracks, and performs the single-leg and over-leg three-point bending mechanical experiments and acoustic emission (AE) tests of composite specimens under 70 °C temperature. The effects of the layup patterns, the loading conditions, and the initial interlaminar crack length on the intralaminar damage and interlaminar delamination behaviors of composite laminates are comparatively studied by analyzing the response process of the AE characteristic parameters including the amplitude, energy, and counting. The AE analysis provides theoretical and technique support for further elucidating the complicated failure mechanisms and their interactions of carbon fiber composite laminates.

**Keywords** Carbon fiber composite laminates · Intralaminar damage and interlaminar delamination · Acoustic emission (AE) test · Single-leg three-point bending (SLB) and over-leg three-point bending (OLB)

## Introduction

Carbon fiber-reinforced resin composites have been increasingly used in areas of the aerospace, mechanical engineering, new energy vehicles, ocean and boats, pressure vessel and piping, wind-power generation, and gas and oil industry due to their excellent properties such as high strength and stiffness-weight-ratios. An important feature of the composites lies in the designability. The composites are generally designed in the form of laminated structures to achieve a good combination of lightweight and high-strength performance. The laminated structures can resist the external loads from different directions due to the different principal fiber orientations for each layer.

For the lightweight design, the conception of structural integrity of composite structures integrates a series of performance including the strength, stiffness, damage tolerance, and lifetime [1]. An important task in process of the design and application of composites is to understand the mechanical properties of composites under various loads and environments, and to evaluate how long the applied composite structures can be used by considering the propagating cracks which can be properly tolerated in the composite structures. It is well known that the failure mechanisms of composites are generally very complicated, which include the matrix cracking, fiber–matrix debonding, fiber breakage, and delamination. In particular, the delamination growth due to the low strength of resin materials that is distinctly characterized by the irreversible

P. F. Liu (✉) · J. Yang · J. Y. Zheng  
Institute of Chemical Machinery and Process Equipment,  
Zhejiang University, Hangzhou 310027, China  
e-mail: pfliu@zju.edu.cn

B. Wang  
Hangzhou Special Equipment Inspection Institute,  
Hangzhou 310003, China

Z. F. Zhou  
Engineering Division, Zhejiang University City College,  
Hangzhou 310015, China

**Fig. 1** Composite specimens under (a) single-leg three-point bending (SLB) and (b) over-leg three-point bending (OLB). Where  $a$  is the crack length,  $L$  is the half span length,  $b$  is the truncation length,  $h/2$  is a half of the specimen thickness, and  $P$  is the external force

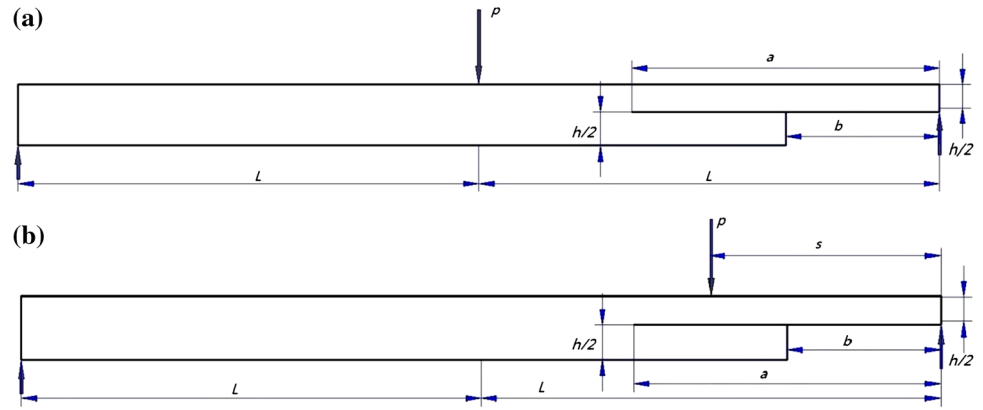


**Table 1** Geometry sizes and layup patterns for four composite specimens

Number	Length × width × thickness (mm)	Initial crack length (mm)	Delaminated interface (mm)	Layup patterns
①	150 × 20 × 3.5	50	25	[0° <sub>16</sub> //0° <sub>16</sub> ]
②	150 × 20 × 3.5	50	25	[30° <sub>16</sub> //30° <sub>16</sub> ]
③	150 × 20 × 3.5	75	37.5	[0° <sub>16</sub> //0° <sub>16</sub> ]
④	150 × 20 × 3.5	50	25	[15°/- 15°] <sub>3s</sub> //[15°/- 15°] <sub>3s</sub>

Where the subscript “s” denotes the symmetry and (“//”) denotes the delaminated interface

crack propagation and energy dissipation, will decrease the stiffness and strengths as well as the structural integrity of composite structures to a large extent [2, 3]. In addition, the interaction between the intralaminar damage and interlaminar delamination is also an important challenging issue.

Currently, some advanced nondestructive inspection technique including the X-ray, ultrasonic and acoustic emission (AE) has been used to explore the damage and failure mechanisms of lightweight composite structures. This test technique develops with the goal of achieving high sensitivity, rapid response speed, and high precision. Especially, the AE is demonstrated to be able to dynamically monitor the damage and failure process of composites through detection of transient wave propagation generated by the rapid energy release in the damaged composites. In general, the AE test whose signals originate from various sources such as matrix cracking, fiber/matrix debonding, fiber breakage, and delamination of composites, attempts to establish the mapping correlations between the failure mechanisms and AE characteristic parameters [4].

For the theoretical methods using the AE technique, the characteristic parameters such as the amplitude [5], the waveforms [6–9], the frequency [10], the clustering [11, 12], and the rise angle [13] are used, respectively, to study the failure mechanisms of composites. Specially, the AE test technique was reviewed by Hamstad [14] in terms of the detection efficiency for quantitative and qualitative estimation for the quality of composites. Fotouhi et al. [15]

**Table 2** Elastic parameters of T700/8911 composites

$E_1$ (GPa)	$E_2$ (GPa)	$E_3$ (GPa)	$G_{12}$ (GPa)	$G_{13}$ (GPa)	$G_{23}$ (GPa)	$\nu_{12}$	$\nu_{13}$	$\nu_{23}$
135	11.41	11.41	7.92	3.792	7.92	0.33	0.49	0.33

Where  $E$ ,  $G$  and  $\nu$  denote the Young’s modulus, shear modulus, and Poisson’s ratio, respectively

**Table 3** Strength parameters for T700/8911 composites

$X_t$ (GPa)	$X_c$ (GPa)	$Y_t$ (GPa)	$Y_c$ (GPa)	$S$ (GPa)
2600	1422	60.3	241	94

Where  $X_t$ ,  $X_c$ ,  $Y_t$ ,  $Y_c$ , and  $S$  represent the longitudinal tensile strength, longitudinal compressive strength, transverse tensile strength, transverse compressive strength, and in-plane shear strength, respectively

used three methods (sentry function, AE energy distribution, and AE count distribution) to investigate the delamination of composite laminates. Oskouei and Ahmadi [16] and de Morais et al. [17] performed the research on the mode-I delamination of composite laminates by AE. Silversides et al. [18] performed the research on the delamination onset in carbon fiber composites by AE. Reeder and Rews [19] and Szekrenyes and Uj [20] performed the mixed-mode bending tests for the delamination crack growth of composites. Fotouhi et al. [21] studied the damage characterization of composites under three-point bending using AE. Bohse [22] explored the micro-failure processes in composites using AE. Salavatian and Smith

[23] studied the damage evolution due to the shear and transverse loading and their effects. Campbell and Mott [24] studied the damage tolerance of composites by AE. Ciampa and Meo [25] proposed a new algorithm for the AE

localization and flexural group velocity determination in anisotropic structures. Hill et al. [26], Scholey et al. [27], and Gutkin et al. [28] explored the failure mechanisms including the matrix cracking and delamination of composite laminates by AE. Furthermore, Czigány [29] proved it possible to correlate the AE features such as the number of events, the amplitude, and energy to the physical properties of composites. Ativitavas and Pothisiri [30], Godin et al. [31], Philippidis et al. [32], and de Oliveira and Marques [33] identified the failure mechanisms by AE and neural network. Recently, Liu et al. [34] performed the tensile experiments and AE tests on the composite laminates with a central hole, and explored the progressive failure properties of carbon fiber composites. Unfortunately, there are still no mature theoretical methods by AE for accurately predicting both the intralaminar and interlaminar failure mechanisms of composites.

In this research, we design and prepare the carbon fiber composite specimens with three layup patterns and initial defects, and performed the single-leg and over-leg three-point bending mechanical experiments and AE tests of composite specimens under 70 °C temperature and room temperature environments, respectively. The intralaminar microscopic damage and mixed-mode delamination

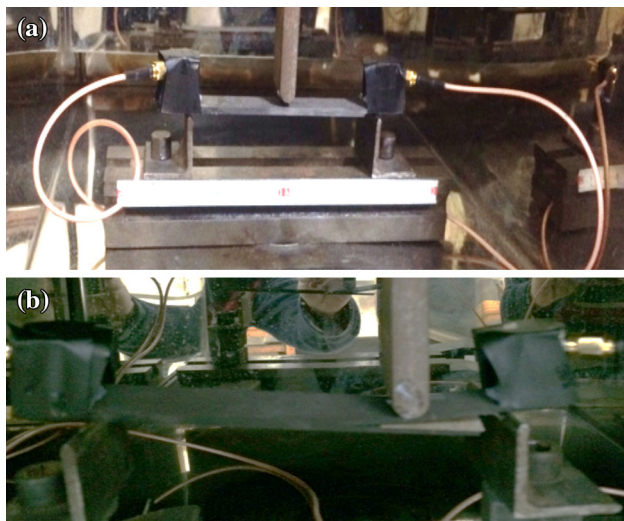
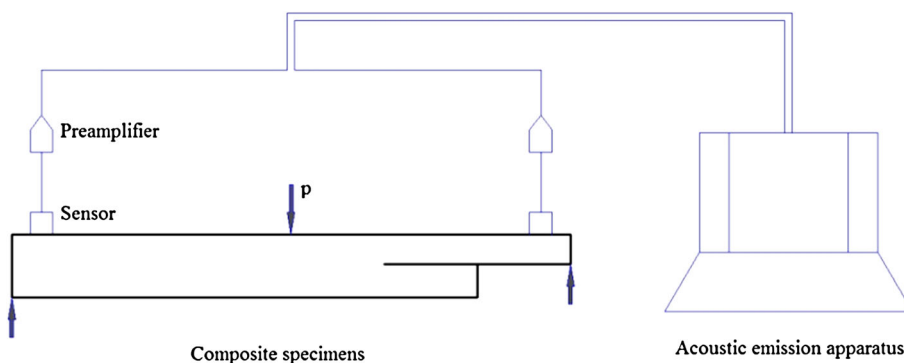


**Fig. 2** Delamination tests: (a) single-leg bending (SLB) and (b) over-leg bending (OLB)

**Fig. 3** High temperature cabinet and high precision temperature controller



**Fig. 4** Schematic description of acoustic emission test system



behaviors of composite laminates with different layup patterns and defect sizes are explored by analyzing the response of the amplitude, energy, and counting.

### Experimental Procedures

#### Material Specimens

The single-leg three-point bending (SLB) and over-leg three-point bending (OLB) specimens are shown in Fig. 1, and the sizes and layup patterns for four composite specimens are listed in Table 1. The material parameters for the unidirectional composites are listed in Tables 2 and 3, respectively. The T700/8911 composite specimens include

three layup patterns  $[0^\circ_{16}/0^\circ_{16}]$ ,  $[30^\circ_{16}/30^\circ_{16}]$ , and  $[15^\circ/-15^\circ]_{3s}/[15^\circ/-15^\circ]_{3s}$ . Each specimen includes 32 layers. The fiber volume fraction of composite is 62%. The initial delaminated interface and the initial crack length are specified.

#### Three-Point Bending Testing

The three-point bending test is performed in the electronic universal test machine (UTM5000) according to the Chinese composite standard “fiber-reinforced plastic composites-determination of flexural properties (Number: GB/T1449-2005)” published in 2005 [35], as shown in Fig. 2. The

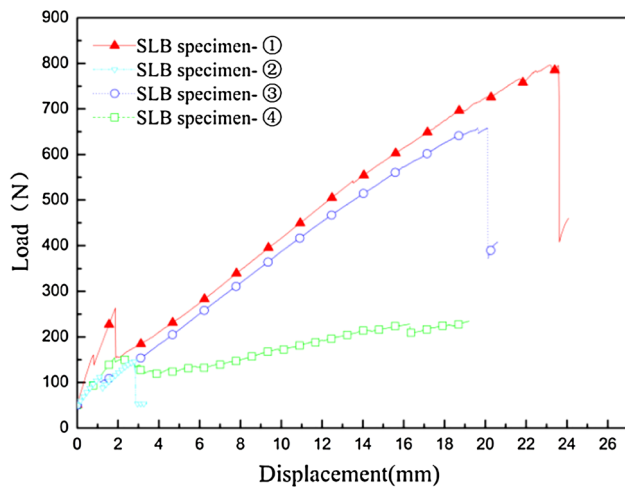


Fig. 5 The load–displacement curves under single-leg bending for four composite specimens

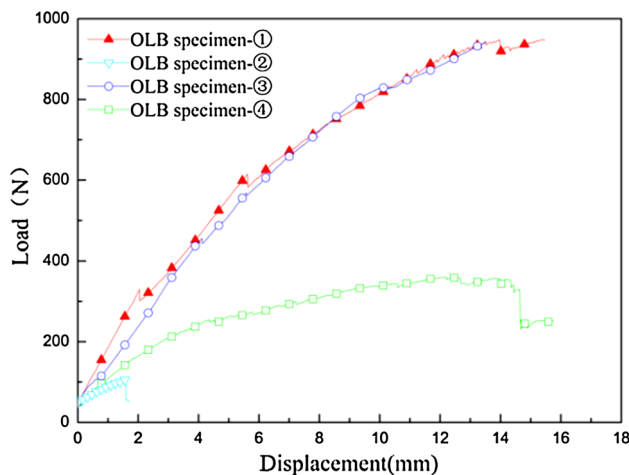


Fig. 6 The load–displacement curves under over-leg bending for four composite specimens

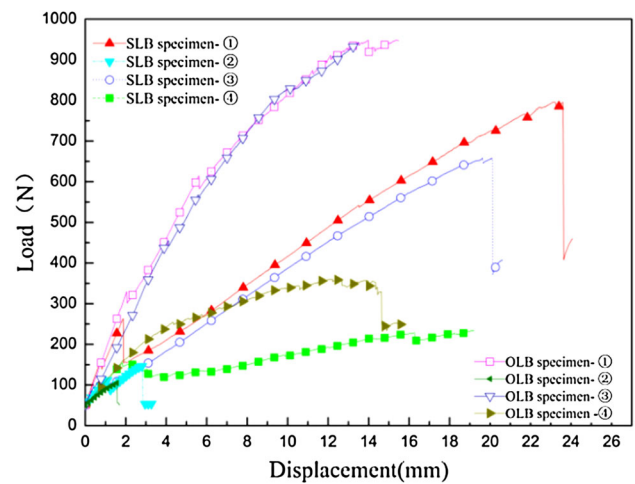


Fig. 7 The load–displacement curves of composites under single-leg bending and over-leg bending under high temperature for eight composite specimens

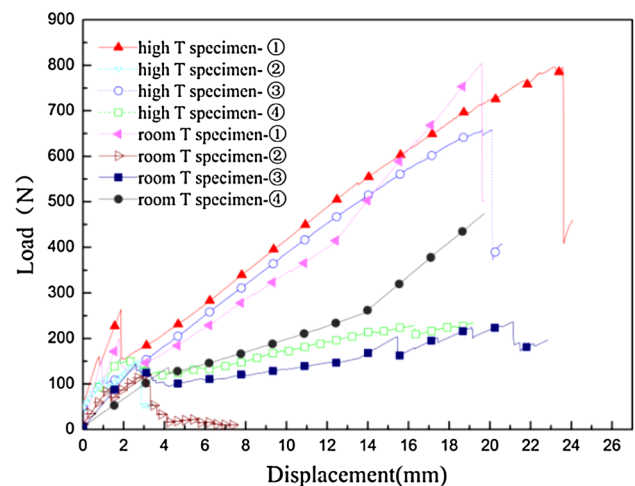
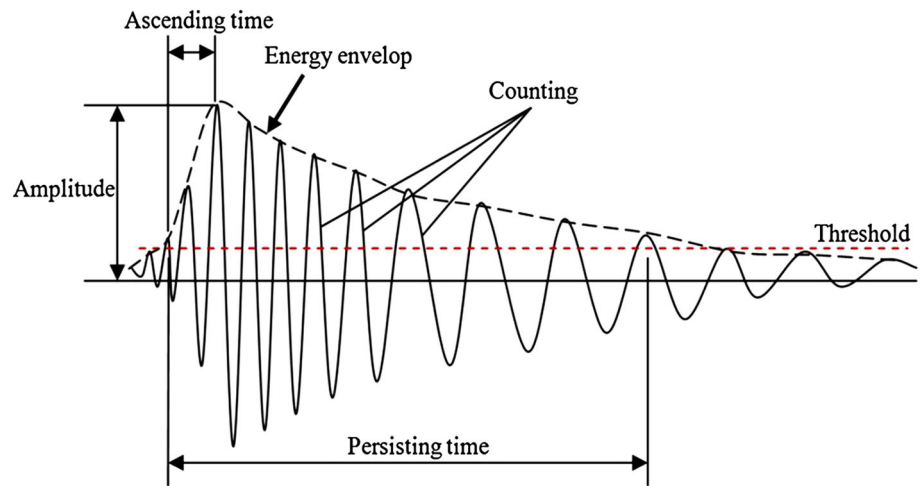


Fig. 8 The load–displacement curves of composites under single-leg bending under high temperature and room temperature for eight composite specimens

**Fig. 9** Schematic description of waveform AE parameters



support span ( $2L$ ) is 112 mm and the load speed is 1.75 mm/min. Before tests, the specimens are placed in the high temperature chamber (as shown in Fig. 3) under 70 °C temperature for 10 min and then loaded up to the collapse of composite specimens.

#### AE Monitoring

The AE equipment is composed of the transducer, the preliminary amplifier, and the PAC Samos-48 AE apparatus including the AE software, and the signal gathering, processing, recording, and display systems, as shown schematically in Fig. 4. The AE tests are performed based on the Chinese spaceflight industry standard “acoustic emission inspection method of composite structures (Number: QJ2914-97)” published in 1997 [36], and the Chinese book “nondestructive inspection technology” [37]. Two piezoelectric transducers are used to search the signal sources of AE activities. In order to improve the acoustic coupling quality between the sensor and the specimens, the high vacuum grease covers the surface of sensors. The signals are detected by the 2/4/6-AST pre-amplifier which employs the enlarging circuits with the frequency range of 50 kHz–2 MHz. The gain selector of the preamplifier is set to 40 dB to filter the noise. The calibration of AE signals is necessary before tests to improve test precision. The attenuation of AE signals is measured by repeating the breakage test of pencil lead for several times at different positions between the AE sensors. During the test, the AE signals are monitored by two sensors according to the difference of the arrival time of the AE signals received by the two transducers. The energy–time curve, the counting–time curve, and the amplitude–time curve are also recorded by the AE software during the test. The timing parameters are: peak definition time

(PDT) = 50  $\mu$ s, hit definition time (HDT) = 200  $\mu$ s, and hit lockout time (HLT) = 300  $\mu$ s.

## Results and Discussion

#### Mechanical Properties of Composite Specimens

Figures 5 and 6 show the load–displacement curves for the single-leg and over-leg three-point bending for four composite specimens, respectively. By comparison, five points can be found: (1) the early damage appears on the border of the initial interlaminar crack arising from severe stress concentrations and the final collapse for all specimens are at the loading end. Load suddenly drops when the delamination crack starts to propagate and the slope of the load–displacement curve decreases until the final collapse; (2) for the specimens with the same layup pattern, at the early stage (0–100 s), the single-leg bending specimen-① and specimen-③ take on different load responses. The specimen-① shows an obvious sudden load drop point, yet for the specimen-③ this feature is not obvious. The reason might be that the initial crack length for the specimen-① is shorter than that for the specimen-③. The SLB test indicates that the critical load reaches the highest value if the crack length exhibits the lowest value [20]. The difference of the initial crack lengths has large effect on the early stage of the tests, but small effect in the late stage of crack propagation; (3) the  $[0^\circ_{16}/0^\circ_{16}]$  specimen shows stronger ability to resist the damage and failure than other two layup patterns when the geometry sizes are the same. In the same way, the  $[30^\circ_{16}/30^\circ_{16}]$  specimens show weaker bending strength than the  $[15^\circ_{-15}]_{3s}/[15^\circ_{-15}]_{3s}$  specimens; (4) Fig. 7 shows the load–displacement curves for eight composite specimens

**Fig. 10** Acoustic emission response of composite specimen-① under single-leg bending under 70 °C temperature: **(a)** counting–time curve, **(b)** energy–time curve, **(c)** amplitude–time curve, and **(d)** amplitude–location curve

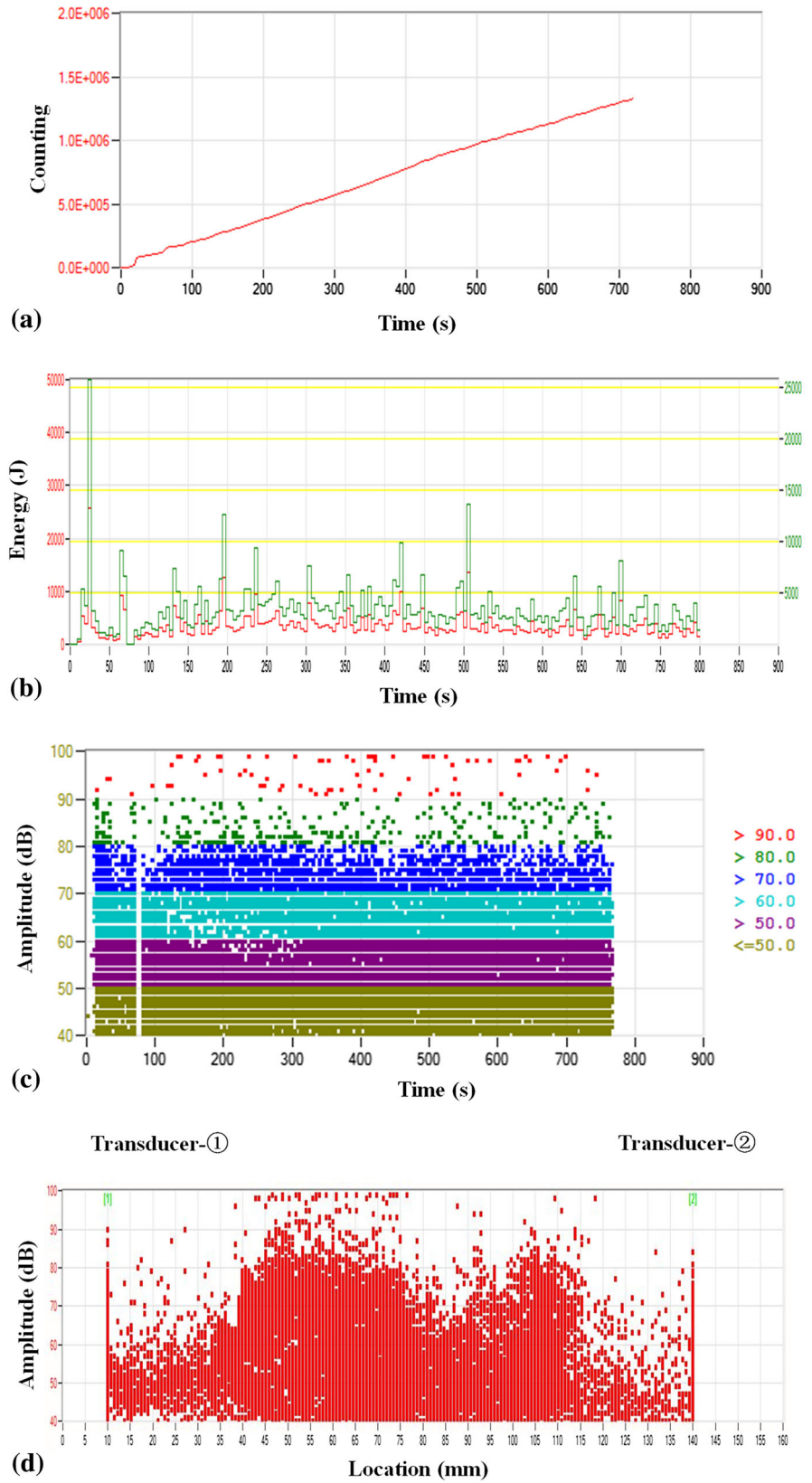


**Fig. 11** Acoustic emission response for the composite specimen-① under single-leg bending under 70 °C temperature: amplitude–location curve at different time

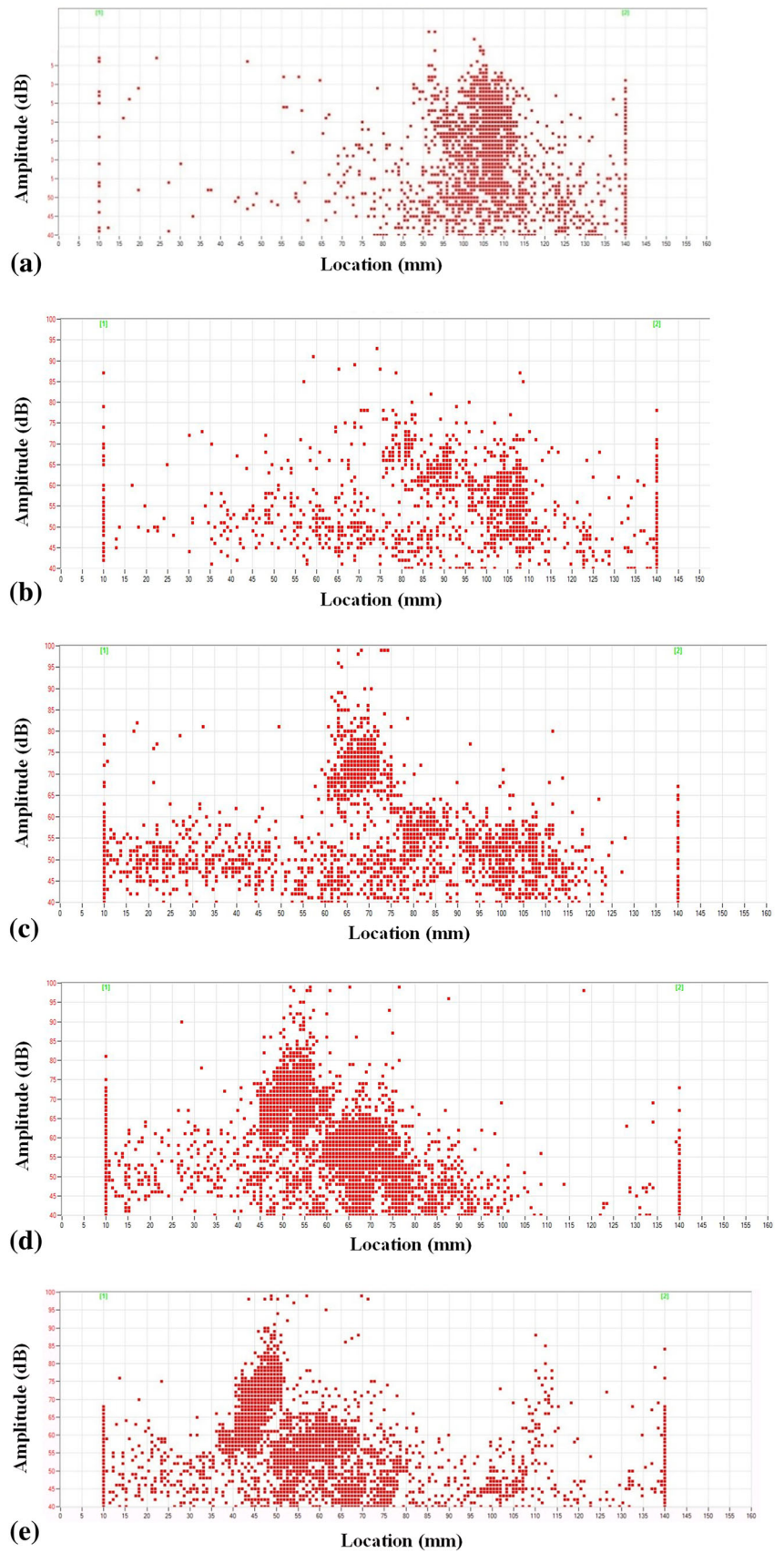
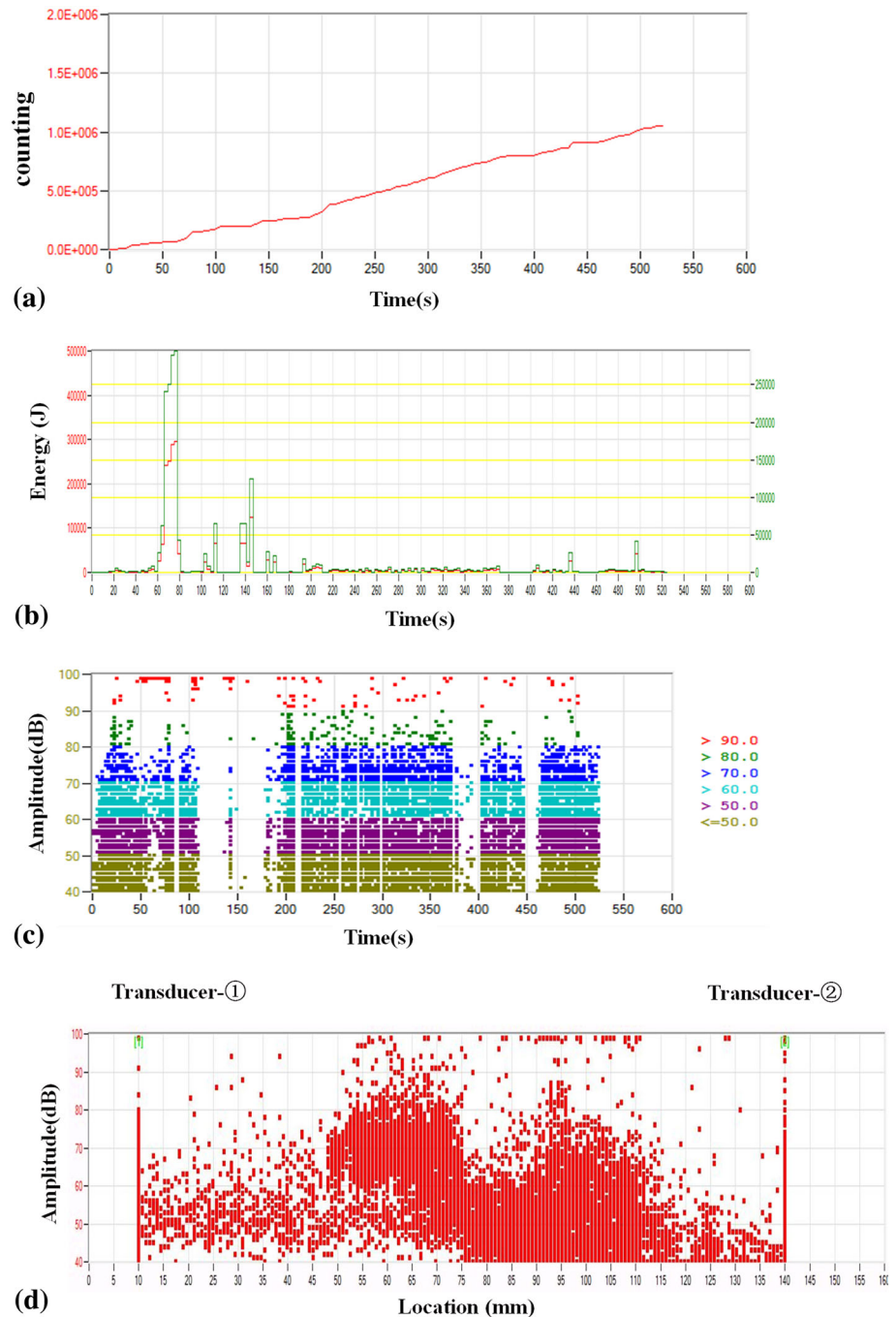


**Fig. 12** Acoustic emission response for the composite specimen-① under over-leg bending under 70 °C temperature: **(a)** counting–time curve, **(b)** energy–time curve, **(c)** amplitude–time curve, and **(d)** amplitude–location curve



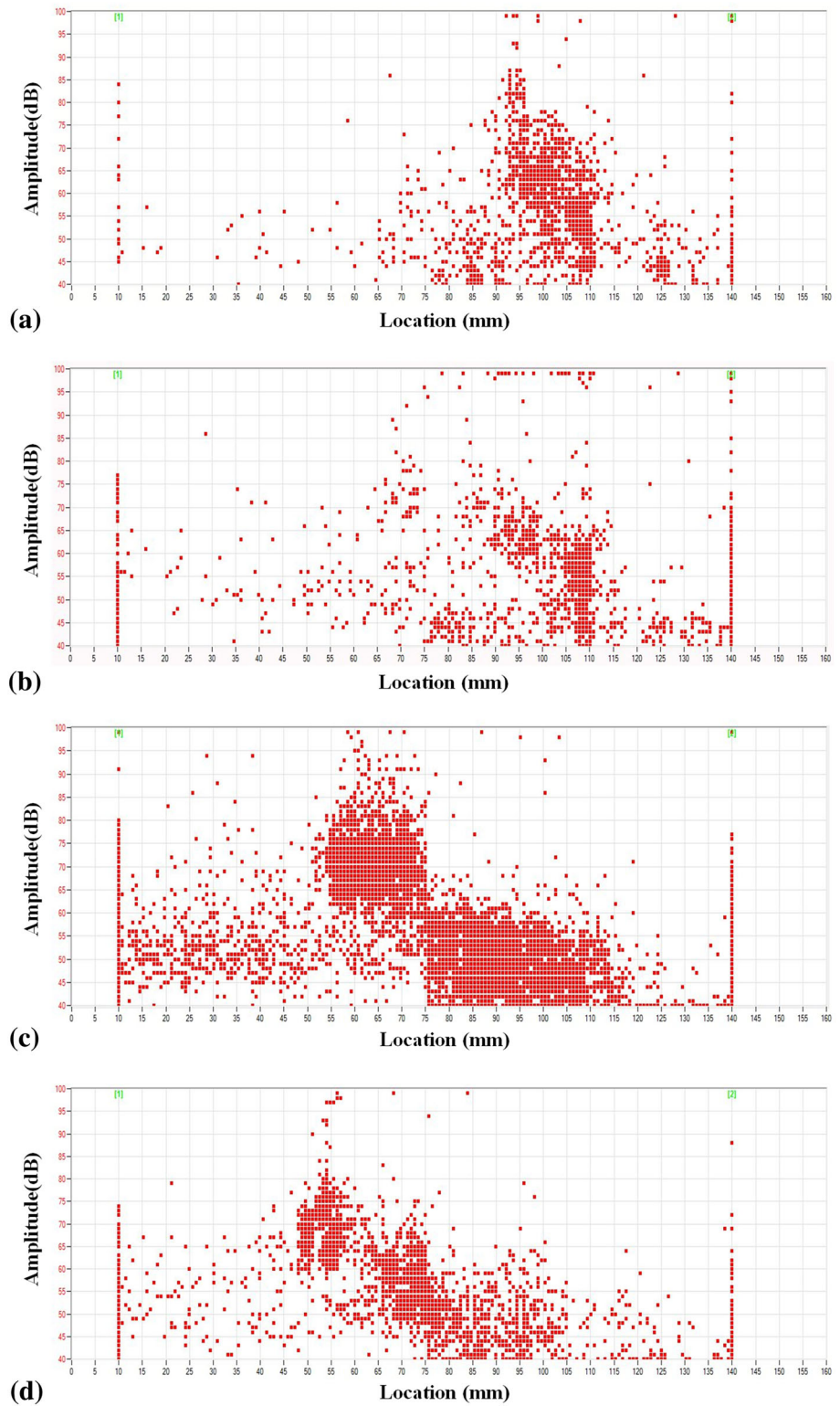
under the single-leg bending and over-leg three-point bending. The over-leg three-point bending specimen shows higher bending strength than the single-leg three-point bending. The crack propagation is prohibited because of smaller bending moment for the over-leg bending; (5) Fig. 8 shows the single-leg bending load–displacement curves under two temperature conditions. It is shown the 8911 resin shows strong ability to resist the 70 °C temperature.

#### AE Feature of Composite Specimen-①

During three-point bending tests of composites, the AE signals are received from the damaged specimens. Fang et al. [38] performed high-fidelity simulation of multiple fracture processes of composite laminates under tensile loads and divided the failure mechanisms into the delamination, splitting crack, transverse matrix cracks, and fiber breakage. In general, the AE amplitude ranges for the



**Fig. 13** Acoustic emission response for the composite specimen-① under over-leg bending: amplitude–location curve at different time



matrix cracking, fiber/matrix interface debonding, delamination, and fiber breakage are about 40–60, 50–70, 60–80, and 80–100 dB, respectively [34, 39]. In Refs. [8, 9, 20], the AE amplitude and energy were used to identify the

failure mechanisms in fiber composites. The schematic description of waveform AE signal parameters is shown in Fig. 9, including mainly three characteristic parameters: energy, counting, and amplitude [37]. In this work, these

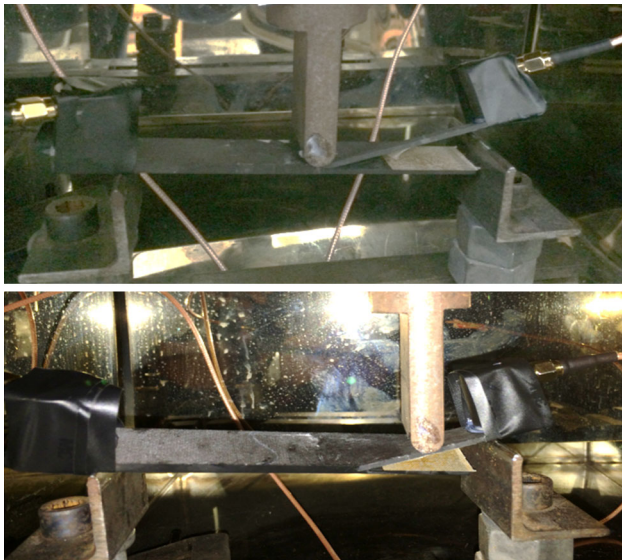


**Fig. 14** The single-leg bending and over-leg bending for the  $[30_{16}/30_{16}]$  specimen under 70 °C temperature

three parameters are used to analyze the failure mechanisms of composites.

Figure 10 shows the AE response in terms of the involvement of energy, counting, and amplitude for the single-leg three-point bending  $[0^{\circ}_{16}/0^{\circ}_{16}]$  specimen under 70 °C temperature. The damage process includes three stages: (1) at the early stage, the energy, counting, and amplitude of AE signals are small, which are consistent with roughly linear deformation behavior. Little matrix cracking with 50–60 dB amplitude signals start to appear. Then, little fiber/matrix debonding, delamination, and fiber breakage with 60–90 dB amplitude signals also emerge; (2) at the middle damage stage, the increasing bending stress leads to the progressive delamination growth and more severe damage, which is represented by more high-amplitude signals, counting, and energy. The main failure is still the matrix cracking, interface debonding and delamination, and little fiber breakage with beyond 80 dB amplitude signals; (3) at the stage of collapse, the low- and middle-amplitude of signals remain the same, the energy decreases little, and the counting adds, which show more fiber breakage with 80–100 dB amplitude signals, and the progressive matrix cracking and interface debonding with the low- and middle-amplitude signals. From the amplitude–location curves, the high-amplitude signals appear between the 45 and 115 mm positions with severe stress concentrations, close to the initial delamination crack.

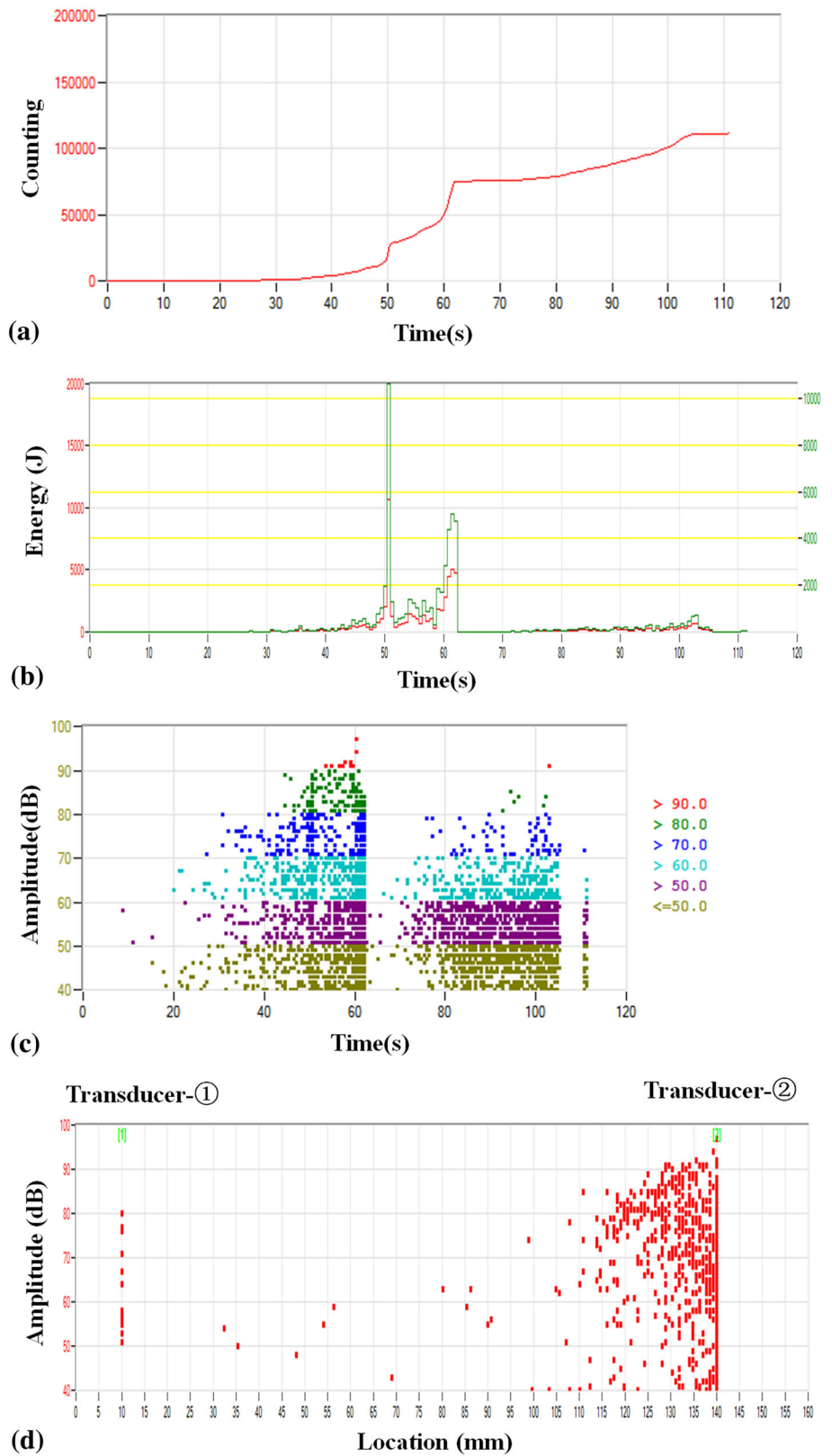
Figure 11a–e shows the amplitude–location curves for the single-leg three-point bending composite specimen  $[0^{\circ}_{16}/0^{\circ}_{16}]$  at different time under 70 °C. However, the case is different for the composite specimens with the layup and initial interlaminar cracks. In Fig. 11a (0–62 s),

many middle- and low-amplitude and few high-amplitude signals concentrate on the area near the initial crack. The high-amplitude signals with beyond 80 dB arise from the fiber breakage and the signals below 70 dB from fiber/matrix debonding, respectively, which all appear at the 90–115 mm position. This is because the deflection is large and the fiber breakage leads to high-amplitude signals near the loading end. The delamination crack propagates from 100 to 90 mm position. As shown in Fig. 11b (62–100 s), the area with 60–80 dB amplitude dense signals moves left to the middle position. The failure modes are mainly fiber/matrix debonding and delamination. The delamination crack propagates from 90 to 75 mm position. As shown in Fig. 11c (100–200 s), the signals with below 60 dB amplitude increase at the 10–60 mm position and aggregates with below 65–90 dB at the 60–75 mm position. The delamination crack propagates from 75 to 60 mm position. As shown in Fig. 11d (200–500 s), the signals with high amplitude move left and the crack propagates to 45 mm position. As shown in Fig. 11e, (500 s-end), the crack propagates to 40 mm position and the specimen collapses. From the theoretical analysis, the delamination crack growth results in the progressive matrix cracking and fiber/matrix debonding and fiber breakage, which leads to the interactions between various failure mechanisms.

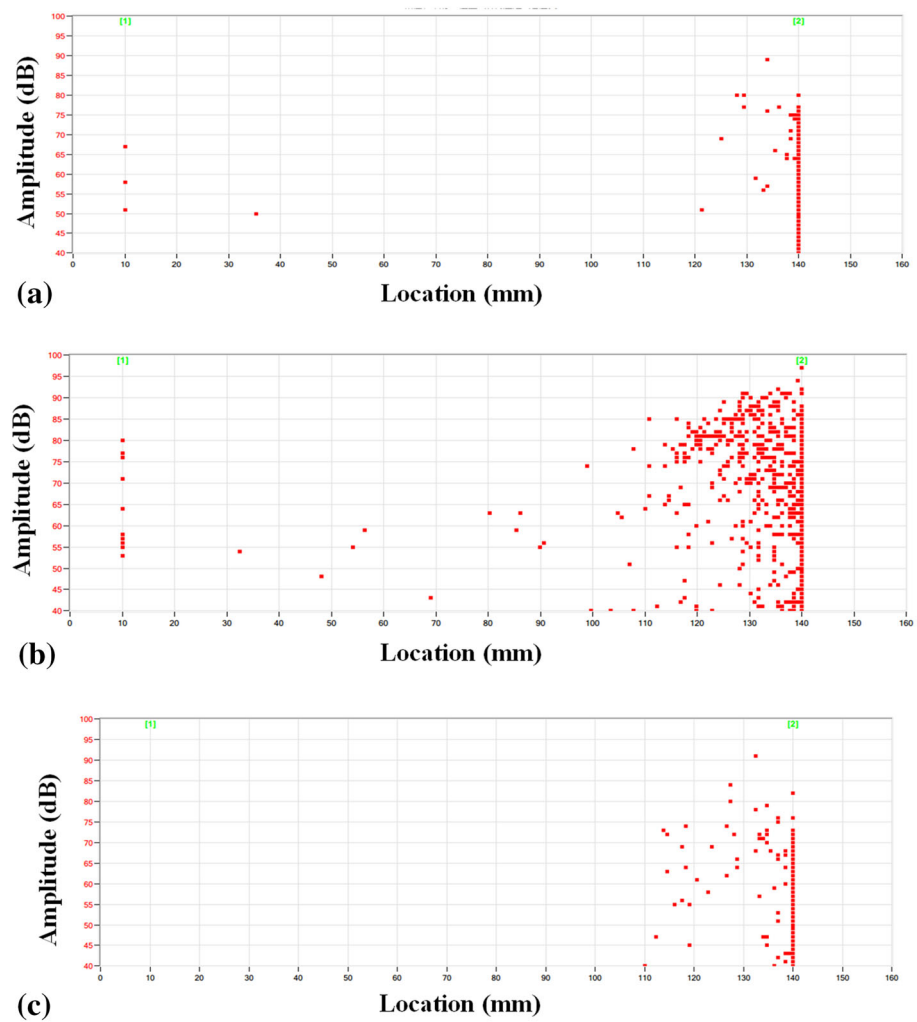
Figure 12 shows the AE response in terms of the involvement of energy, counting, and amplitude for the over-leg three-point bending  $[0^{\circ}_{16}/0^{\circ}_{16}]$  specimen under 70 °C temperature. The analytical solutions on the delamination fracture toughness and mechanical properties for the SLB specimen and OLB were derived by Szekrenyes and Uj [20]. In general, the amplitude signals for the over-leg specimens are more than those for the single-leg specimens. In addition, the over-leg specimens show more counting and more complicated delamination properties. The damage evolution includes three stages: (1) at the early stage, the energy, counting, and amplitude are few; (2) at the middle stage, the matrix cracks and delamination cracks propagate with high amplitude, indicating more severe damage area. At the same time, some signals with beyond 90 dB amplitude start to appear; and (3) at the stage of collapse, the signals with middle- and low-amplitude become constant and the signals with 80–100 dB amplitude add, showing more matrix cracking, fiber/matrix debonding, delamination, and few fiber breakage. From the amplitude–location curves, the high-amplitude signals locate at the 50–100 mm position.

Figure 13a–d shows the amplitude–location curves for the  $[0^{\circ}_{16}/0^{\circ}_{16}]$  composite specimens under over-leg three-point bending at different time under 70 °C temperature. As shown in Fig. 13a (0–70 s), many signals with middle-

**Fig. 15** Acoustic emission response for the composite specimen-② under single-leg bending under 70 °C temperature: **(a)** counting–time curve, **(b)** energy–time curve, **(c)** amplitude–time curve, and **(d)** amplitude–location curve



**Fig. 16** Acoustic emission response for the composite specimen-② under single-leg bending under 70 °C temperature: amplitude–location curves at different time



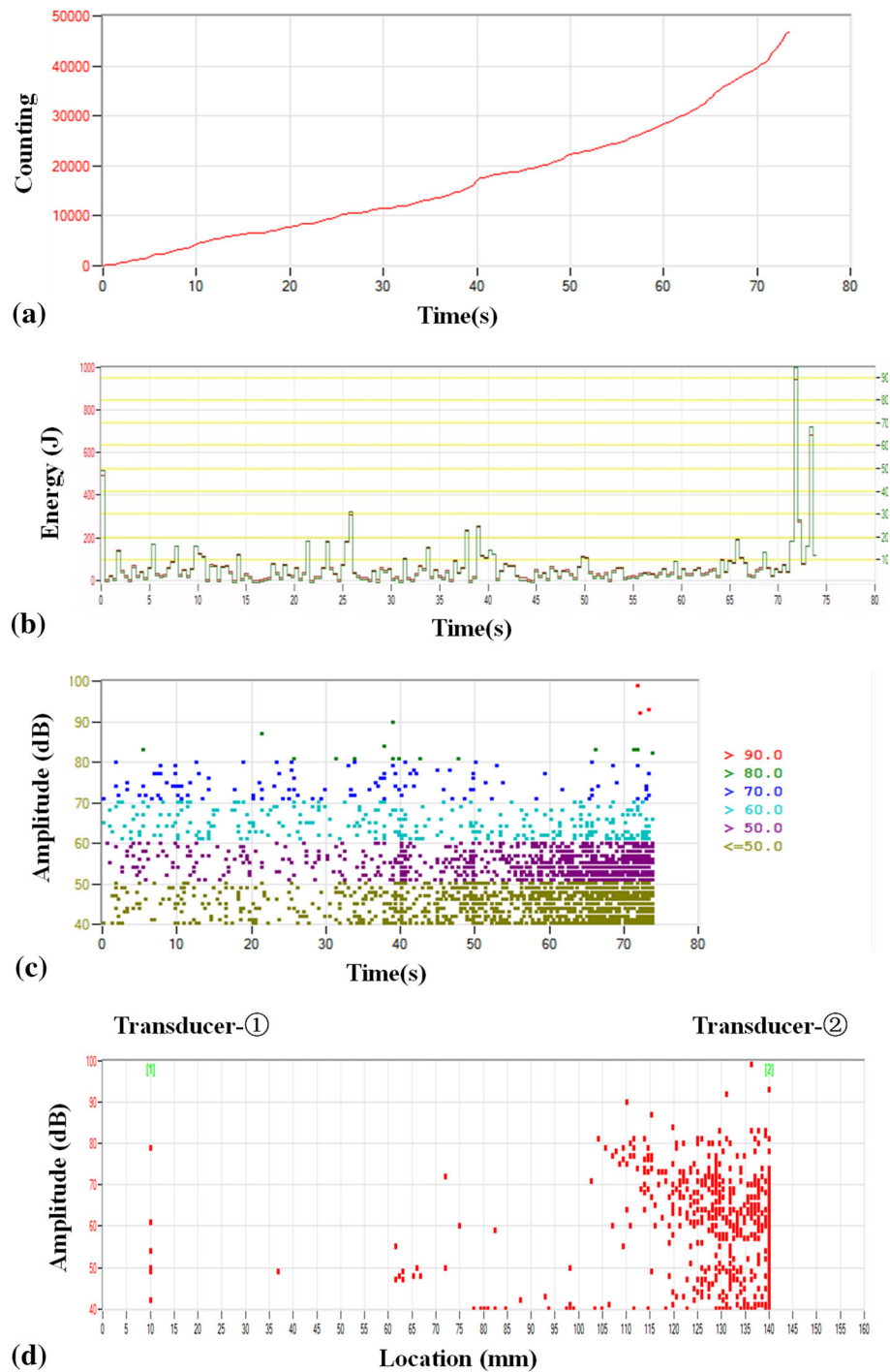
and low-amplitude and few signals with beyond 80 dB amplitude concentrate on the area near the loading end and initial crack. The crack propagates from 100 to 92 mm position. As shown in Fig. 13b (70–200 s), many signals with middle- and low-amplitude and few high-amplitude signals appear at the 70–110 mm position. The failure modes are the matrix cracking, fiber/matrix debonding, delamination, and fiber breakage. As shown in Fig. 13c (200–420 s), the signals with below 75, 100, and 60 dB amplitude appear at the 10–55, 55–75, and 75–115 mm, respectively, corresponding to the interface debonding, fiber breakage, and matrix cracking. The crack propagates from 75 to 55 mm position. As shown in Fig. 13d (420 s-end), the signals move left and the specimen collapses. It is concluded from the analysis above after the continuous delamination crack growth, only upper sublaminate resists the bending loads. Thus, more fiber breakage with high-amplitude signals and matrix cracking with middle-amplitude signals appear, showing the rapid

decrease of the load-bearing ability of composite structures due to the delamination.

#### AE Feature of Representation Composite Specimen-②

Figure 14 shows the single-leg and over-leg three-point bending for the  $[30^{\circ}_{16}/30^{\circ}_{16}]$  specimens under 70 °C temperature. Figure 15 shows the corresponding AE response about the evolvement of energy, counting, and amplitude. The  $[30^{\circ}_{16}/30^{\circ}_{16}]$  specimens show fewer signals than other two specimens. The damage process includes three stages: (1) at the early stage, few matrix cracking with 50–60 dB amplitude appears; (2) at the middle stage, the signals with 80–90 dB amplitude add rapidly and the energy reaches the maximum at 50 s; (3) at the stage of collapse, the signals with beyond 90 dB amplitude decrease. From the amplitude–location curves, many signals concentrate on the 115–140 mm positions. Figure 16a–c shows the AE response for the amplitude–

**Fig. 17** Acoustic emission response for the composite specimen-② under over-leg bending under 70 °C temperature: (a) counting–time curve, (b) energy–time curve, (c) amplitude–time curve, and (d) amplitude–location curve



location curve at different time under 70 °C temperature. As shown in Fig. 16b (40–100 s), the delamination cracks start to propagate. The signals with below 65 dB amplitude appear at the initial crack and the dense signals with 70–95 dB amplitude appear at the 110–140 mm position. It is shown that the composite laminate starts to damage along the 30° layup direction in the form of few fiber

breakage. As shown in Fig. 16c (100–110 s), the signals become sparse, showing the lose of the loading–bearing ability of laminates.

Figure 17 shows the AE response in terms of the evolvement of energy, counting, and amplitude for the over-leg three-point bending [30°<sub>16</sub>//30°<sub>16</sub>] specimen under 70 °C temperature. Compared with the single-leg loading,

**Fig. 18** Acoustic emission response for the composite specimen-② under over-leg bending under 70 °C temperature: amplitude–location curves at different time

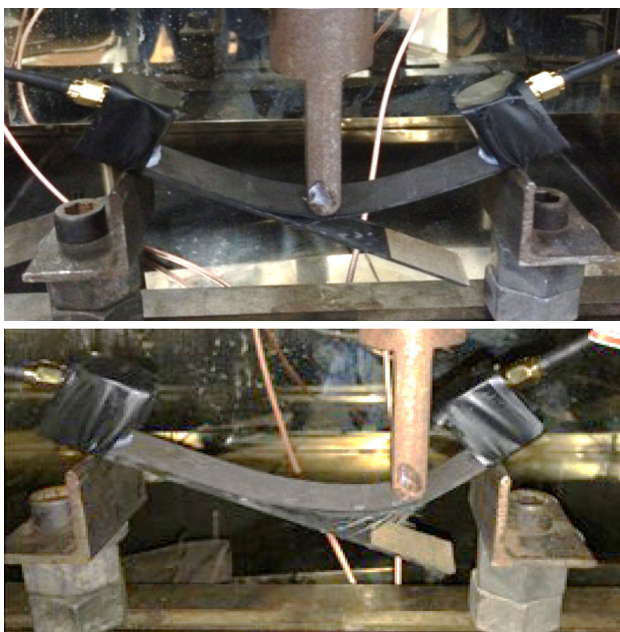
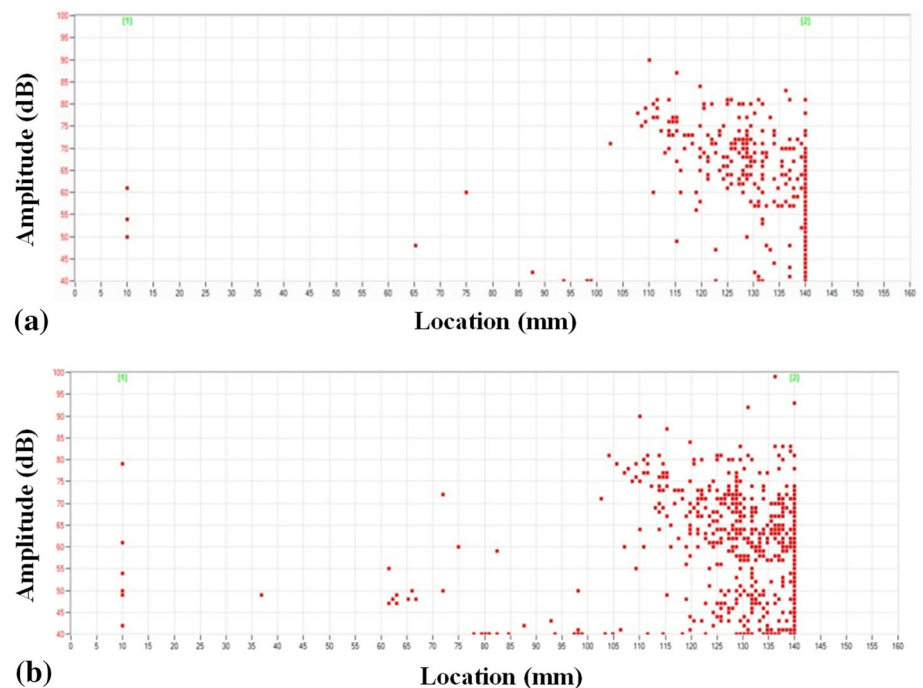


**Fig. 19** The single-leg bending and over-leg bending for the composite specimen-④ under 70 °C temperature

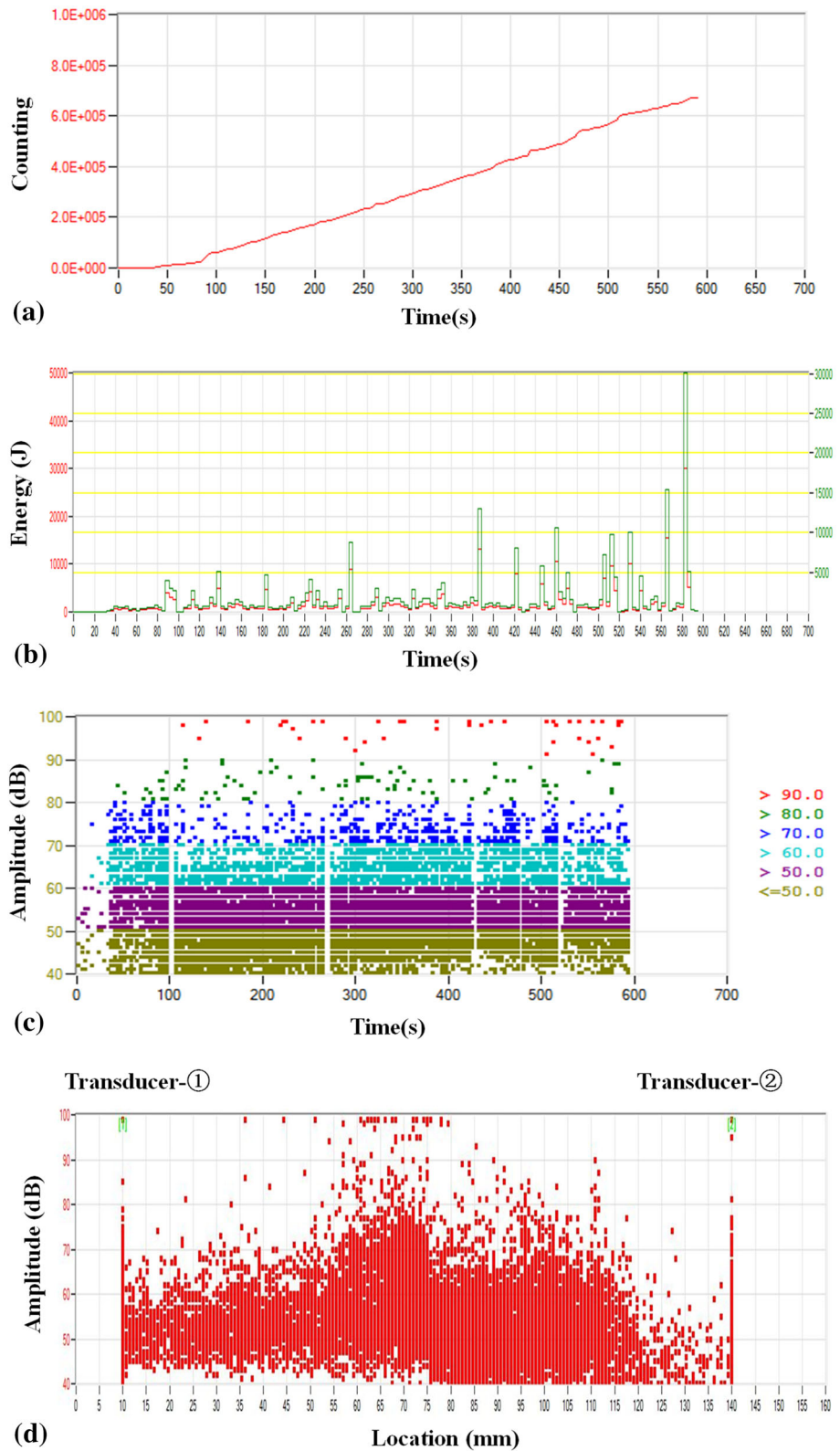
more specimens are completely broken under the over-leg loading. The reason is that the over-leg loading cross head is closer to the right end bearing, which leads to larger right deflection. In this situation, the specimens are subjected to unbalanced forces and most of the forces concentrate on the right. The damage process includes two stages: (1) at the early stage, the energy and counting are few, and the signals with below 80 dB amplitude appear, different from

the single-leg loading; (2) at the second stage, the signals with 40–60 dB amplitude become more dense, but the signals with 60–80 dB amplitude become sparse. The energy rate reaches the maximum at 72 s. From the amplitude–location curves, many signals with below 80 dB and few signals with beyond 80 dB concentrate on the 110–140 mm position. Figure 18a, b shows the AE response for the amplitude–location curves for the over-leg three-point bending  $[30^{\circ}_{16}/30^{\circ}_{16}]$  specimens at different time under 70 °C temperature. As shown in Fig. 18a (0–46 s), only few signals with 40–85 dB amplitude appear at the 105–140 mm position. As shown in Fig. 18b (46 s-end), some signals with 60–85 dB amplitude appear at the 105–140 mm position. From the analysis above, the laminate starts to fracture along the layup direction before the delamination. Different from the single-leg loading, the loading end is close to the initial crack, which leads to larger deflection and damage. The collapse for the over-leg specimens appears at the loading end, and for the single-leg specimens appears at the left side of loading end.

#### AE Feature of Composite Specimen-④

Figure 19 shows the single-leg bending and over-leg three-point bending for the  $[15^{\circ}/-15^{\circ}]_{3s}/[15^{\circ}/-15^{\circ}]_{3s}$  specimens under 70 °C temperature. Figure 20 shows the corresponding AE response about the evolvement of energy, counting, and amplitude. Different from the unidirectional specimens, more complicated delamination behaviors before the 15° layer and –15° layer appear. The damage process includes three stages: (1) at the early stage,

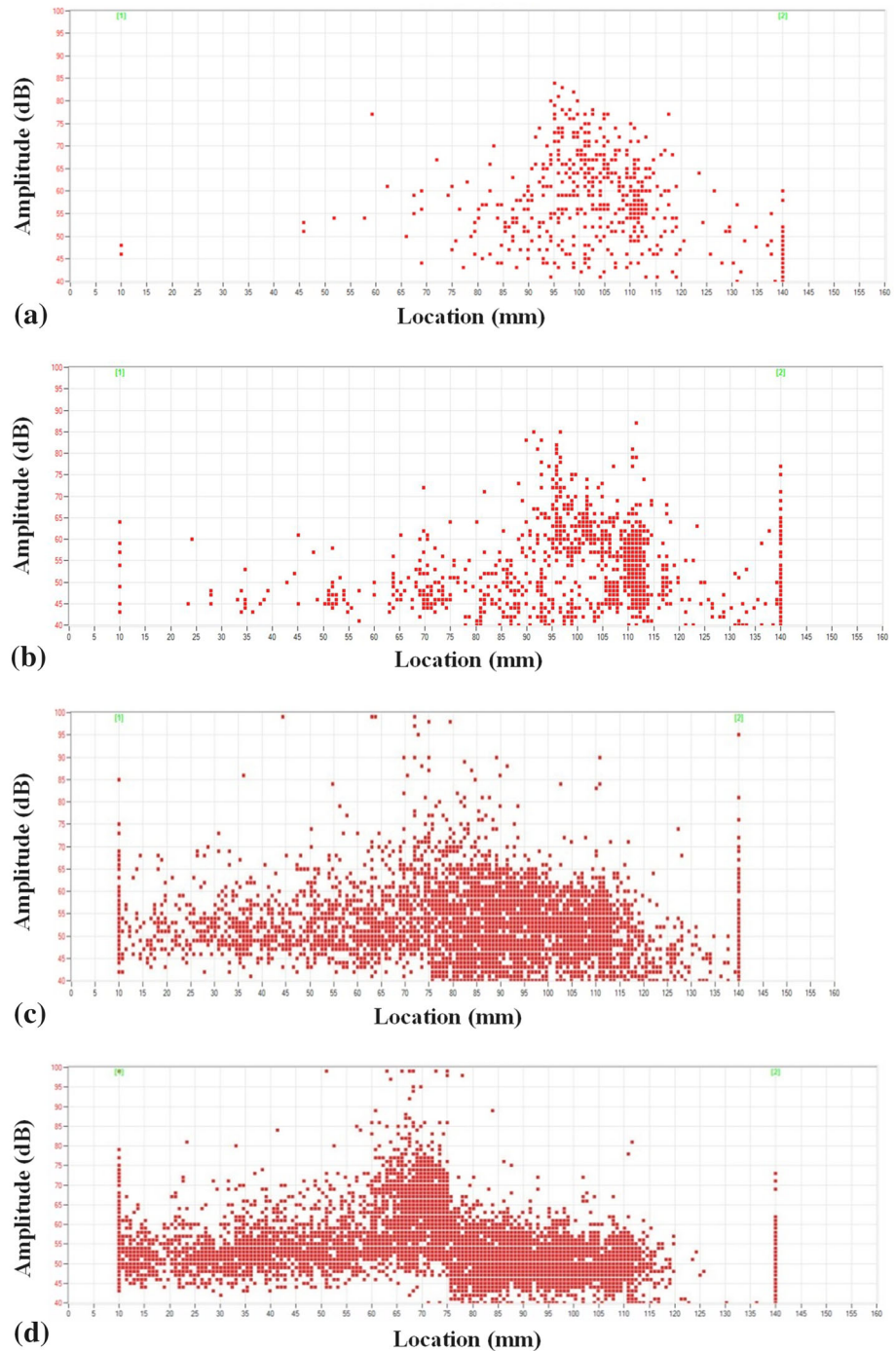
**Fig. 20** Acoustic emission response for the composite specimen-④ under single-leg bending under 70 °C temperature: **(a)** counting–time curve, **(b)** energy–time curve, **(c)** amplitude–time curve, and **(d)** amplitude–location curve



only few signals with 40–70 dB amplitude appear; (2) at the middle stage, the decreasing curve starts to appear after delamination crack growth. More signals with 40–80 dB

amplitude and few signals with 80–100 dB amplitude appear. Besides, the energy and counting also add, showing more damage area; (3) at the stage of collapse, the

**Fig. 21** Acoustic emission response for the composite specimen-④ under single-leg bending under 70 °C temperature: amplitude–location curve at different time



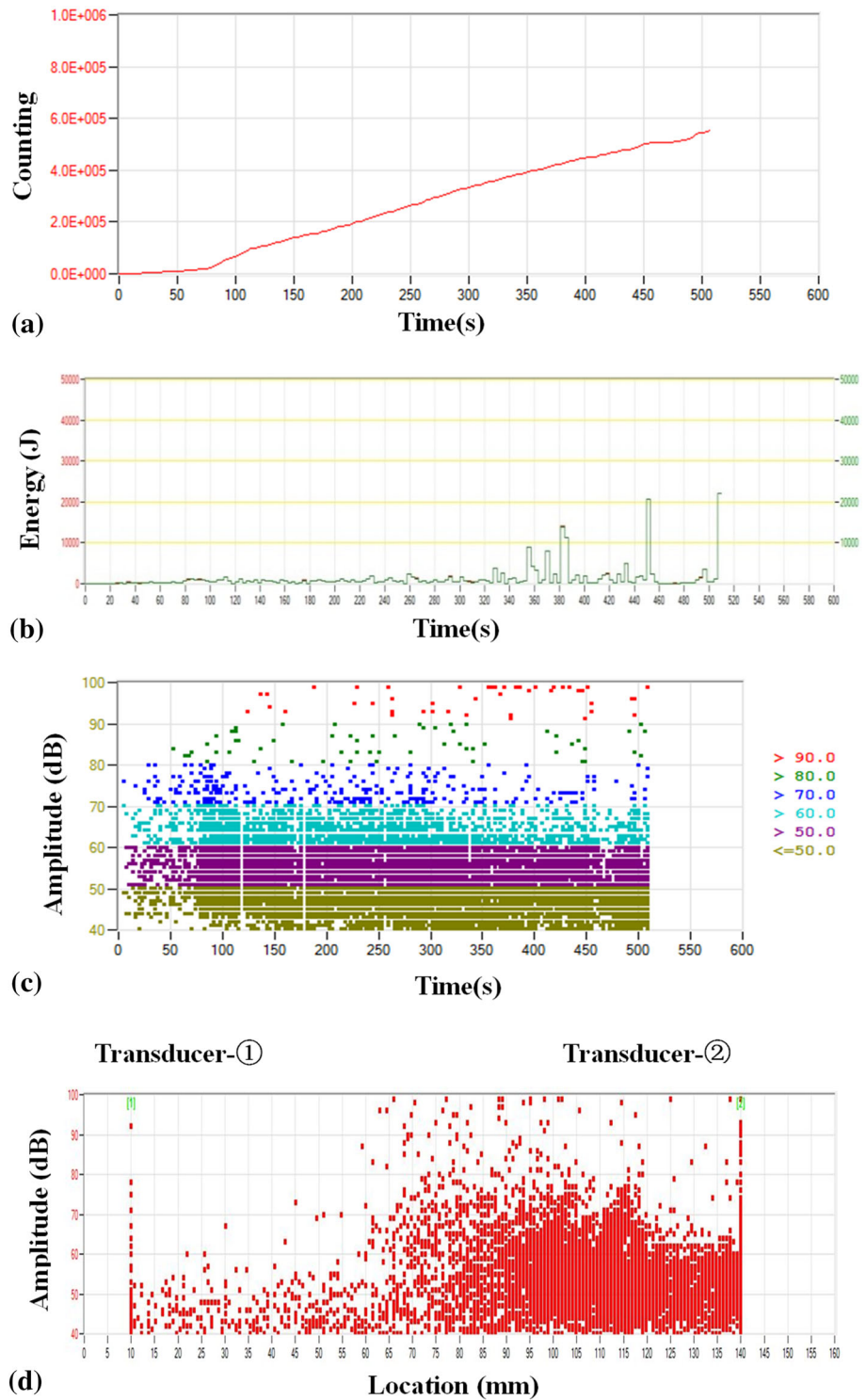
amplitude signals become unchanged and the energy rate reaches the maximum at 520 s. From the amplitude–location curves, many amplitude signals locate at the 10–115 mm position and dense signals aggregate at the loading end.

Figure 21a–e shows the amplitude–location curves for the  $[15^\circ/-15^\circ]_{3s}/[15^\circ/-15^\circ]_{3s}$  specimen under the single-leg three-point bending at different time under 70 °C

temperature. As shown in Fig. 21b (65–100 s), many signals with 40–70 dB amplitude at the 90–115 mm position and few signals with 70–85 dB and below 65 dB amplitude at the left of specimens appear, showing the delamination crack starts to propagate. As shown in Fig. 21c (100–260 s), many signals with below 70 dB amplitude at the 10–115 mm and few signals with 70–100 dB and below 65 dB amplitude appear. Few high-amplitude



**Fig. 22** Acoustic emission response for the composite specimen-④ under over-leg bending under 70 °C temperature: **(a)** counting–time curve, **(b)** energy–time curve, **(c)** amplitude–time curve, and **(d)** amplitude–location curve

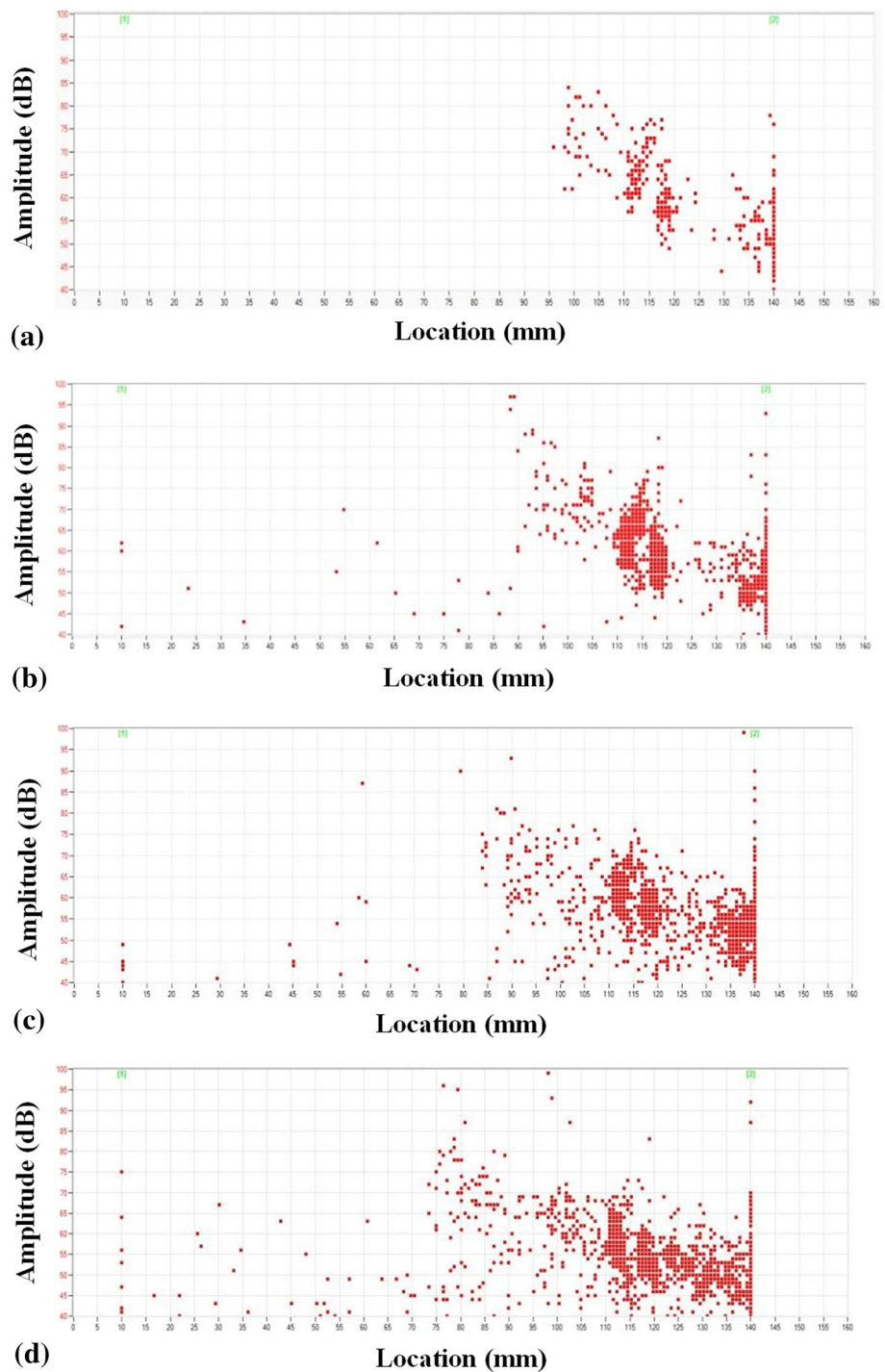


signals mean only few fiber breakage. As shown in Fig. 21d (260–480 s), the high-amplitude signals move left to the 60–75 mm position. The crack propagates to the 60 mm position. As shown in Fig. 21e (480 s-end), the

high-amplitude signals move left to the 50–65 mm and the fiber breakage adds at the loading end.

Figure 22 shows the AE response in terms of the evolution of energy, counting, and amplitude for the

**Fig. 23** Acoustic emission response for the composite specimen-④ under over-leg bending under 70 °C temperature: amplitude–location curve at different time



over-leg three-point bending  $[15^\circ-15^\circ]_{3s} // [15^\circ-15^\circ]_{3s}$  specimen under 70 °C temperature. Figure 23a–f shows the amplitude–location curve at different time. As shown in Fig. 23a (0–70 s), different from the unidirectional specimens, the dense signals appear at the right side of loading end. As shown in Fig. 23b (70–140 s), the signals with 45–80 dB amplitude appear at the 95–140 mm position. The crack propagates to the 90 mm position and the

propagating speed is slow. As shown in Fig. 23c (140–220 s), the signals with below 80 dB amplitude appear at the 85–140 mm position and the crack propagates to the 85 mm position. As shown in Fig. 23d (220–290 s), the signals concentrate on the 70–140 mm position and the crack propagates to the 75 mm position. As shown in Fig. 23e (290–480 s), many signals with below 70 dB amplitude at the 65–140 mm position and few signals with

Fig. 23 continued

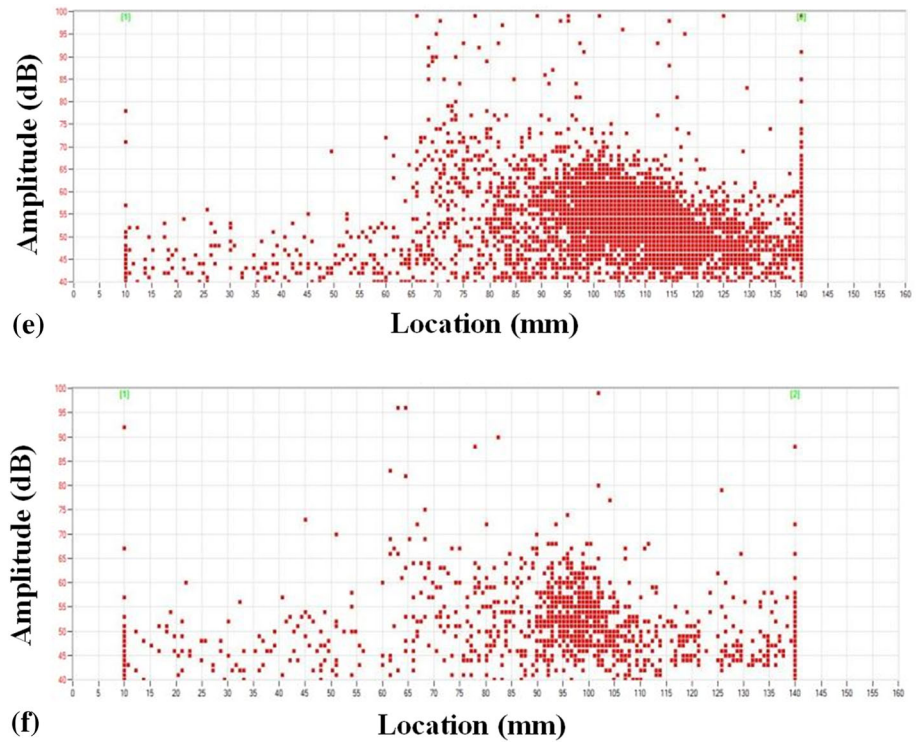
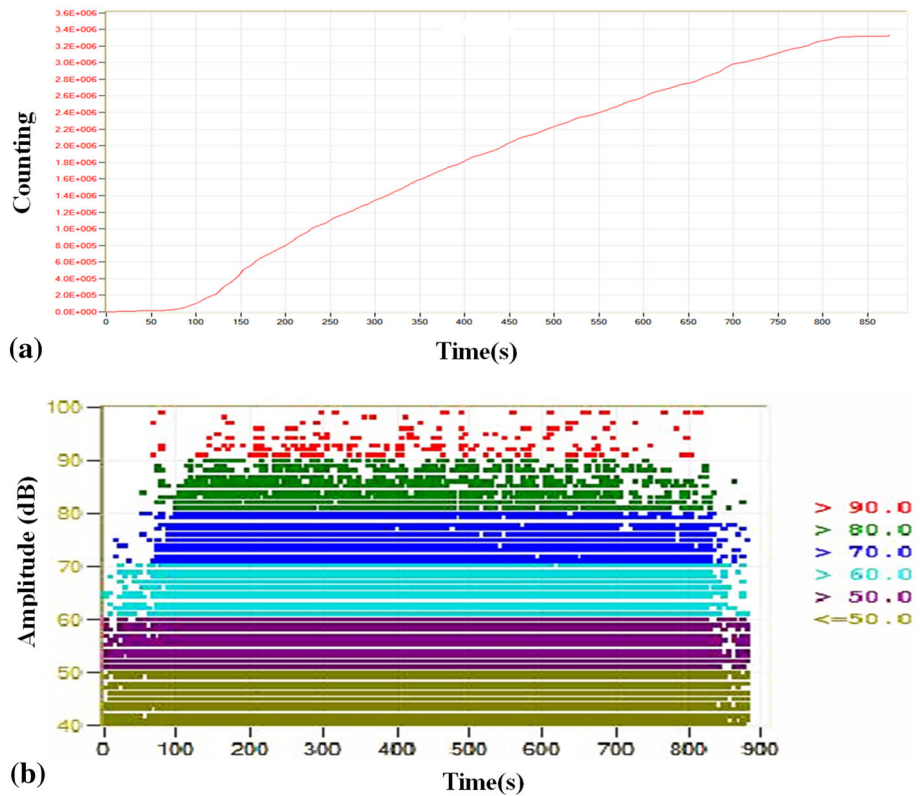
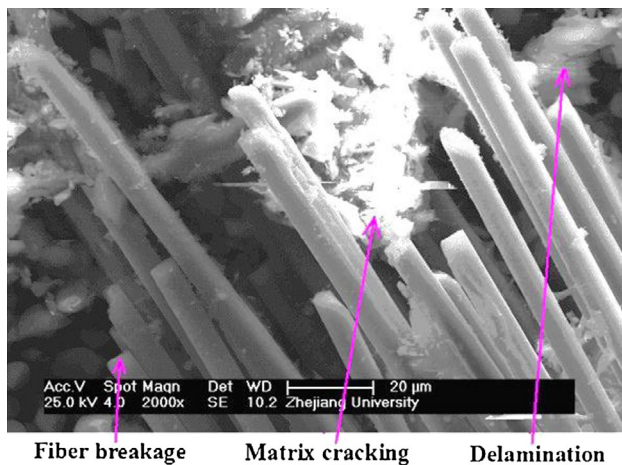


Fig. 24 Acoustic emission response for the composite specimen-① under single-leg bending: (a) counting–time curve and (b) amplitude–time curve



80–100 dB amplitude, and few signals with 55 dB amplitude at the 10–65 mm position appear. The crack propagates to the 65 mm position. As shown in Fig. 23f

(480 s-end), the high-amplitude signals decrease and the amplitude of signals become unchanged. From the fracture specimens, the fiber breakage is sparsely distributed at two



**Fig. 25** The microscopic failure mechanisms of the fracture specimens using scanning electronic microscope

sides of loading end and the area between the loading end and propagating crack tip. The angle-ply specimens are shown to resist the crack propagation and fiber fracture more strongly than the unidirectional specimens.

#### AE Feature of Composites Specimen-① Under Room Temperature

Figure 24 shows the AE response in terms of the evolution of counting and amplitude for the  $[0^\circ_{16}/0^\circ_{16}]$  specimen under the single-leg three-point bending under room temperature. Compared with Fig. 10, two points are obtained: (1) at the early stage, the counting and energy under room temperature are fewer than the specimens under  $70^\circ\text{C}$  temperature, showing more severe damage due to high temperature; (2) at the next stage, the signals with 80 dB amplitude and counting for the specimens under room temperature are more than those under  $70^\circ\text{C}$  temperature, which means more fiber breakage under room temperature appears than under  $70^\circ\text{C}$  temperature. Figure 25 shows the microscopic failure mechanisms of the fracture specimens using scanning electronic microscope. It is shown that the distinct failure mechanisms are: fiber breakage, delamination, and matrix cracking.

## Conclusions

This research performs the single-leg and over-leg three-point bending experiments and AE test of carbon fiber composite laminates under  $70^\circ\text{C}$  temperature and room temperature environments. The initial intralaminar and interlaminar defects are set to activate the interactions of various failure mechanisms. The AE characteristic parameters including the amplitude, counting, and energy

are used to identify the dominating failure modes. Effects of three layup patterns and two initial crack sizes on the delamination behaviors are studied.

From the signal analysis, the following conclusions are obtained:

- (1) The bending strengths for the  $[30^\circ_{16}/30^\circ_{16}]$  and  $[15^\circ/-15^\circ]_{3s}/[15^\circ/-15^\circ]_{3s}$  specimens are smaller than those for the unidirectional  $[0^\circ]$  specimens. Besides, the position of crack-tip can be approximately determined by the signals with beyond 80 dB for the  $[0^\circ_{16}/0^\circ_{16}]$  specimens. Yet, this method cannot be suitable for the  $[15^\circ/-15^\circ]_{3s}/[15^\circ/-15^\circ]_{3s}$  specimens, which can prohibit the fiber breakage in process of delamination effectively in view of the angle-ply layup. By comparison, the  $[30^\circ_{16}/30^\circ_{16}]$  specimens can easily fracture before the delamination under the single-leg loading. Thus, the angle-ply layup pattern helps to improve the mechanical properties of composite laminates.
- (2) The over-leg loading leads to larger bending strength than the single-leg loading for the same specimens. The delamination crack under the single-leg loading propagates more quickly than the over-leg loading. The nonlinear load response is mainly represented by the delamination with 60–80 dB amplitude, the fiber/matrix delamination with 50–70 dB amplitude and the matrix cracking with 40–60 dB amplitude, yet the fiber breakage with the 80–100 dB amplitude is few. The initial delamination crack and progressive delamination growth aggravate the intralaminar damage. Finally, the 8911 resin shows good performance under  $70^\circ\text{C}$  temperature environment.

**Acknowledgments** The author Dr. Pengfei Liu would sincerely like to thank the support by the National Natural Science Funding of China (No.51375435), and the National Key Fundamental Research and Development Project (973 Project, No. 2015CB057603), the Natural Science Funding of Zhejiang Province of China (No. LY13E050002) and the Aerospace Support Technique and Innovation Funding.

## References

1. P.W.R. Beaumont, On the problems of cracking and the question of structural integrity of engineering composite materials. *Appl. Compos. Mater.* **21**(1), 5–43 (2014)
2. P.F. Liu, S.J. Hou, J.K. Chu, X.Y. Hu, C.L. Zhou, Y.L. Liu, J.Y. Zheng, A. Zhao, L. Yan, Finite element analysis of postbuckling and delamination of composite laminates using virtual crack closure technique. *Compos. Struct.* **93**(6), 1549–1560 (2011)
3. P.F. Liu, J.Y. Zheng, On the through-the-width multiple delamination, and buckling and postbuckling behaviors of symmetric

- and unsymmetric composite laminates. *Appl. Compos. Mater.* **20**(6), 1147–1160 (2013)
4. S. Benmedakhene, M. Kenane, M.L. Benzeggagh, Initiation and growth of delamination in glass/epoxy composites subjected to static and dynamic loading by acoustic emission monitoring. *Compos. Sci. Technol.* **59**(2), 201–208 (1999)
  5. X.M. Zhuang, X. Yan, Investigation of damage mechanisms in self-reinforced polyethylene composites by acoustic emission. *Compos. Sci. Technol.* **66**(3–4), 444–449 (2006)
  6. R.T. Bocchieri, R.A. Schapery, M.R. Gorman, Time-dependent microcracking detected in a rubber-toughened carbon–epoxy composite by the modal acoustic emission method. *J. Compos. Mater.* **37**(5), 421–451 (2003)
  7. Y.A. Dzenis, J. Qian, Analysis of microdamage evolution histories in composites. *Int. J. Solids Struct.* **38**(10), 1831–1854 (2001)
  8. M. Johnson, G. Peter, Broad-band transient recording and characterization of acoustic emission events in composite laminates. *Compos. Sci. Technol.* **60**(15), 2803–2818 (2000)
  9. S. Huguet, N. Godin, R. Gaertner, L. Salmon, D. Villard, Use of acoustic emission to identify damage modes in glass fibre reinforced polyester. *Compos. Sci. Technol.* **62**(10), 1433–1444 (2002)
  10. C.R. Ramirez-Jimenez, N. Papadakis, N. Reynolds, T.H. Gan, P. Purnell, M. Pharaoh, Identification of failure modes in glass/polypropylene composites by means of the primary frequency content of the acoustic emission event. *Compos. Sci. Technol.* **64**(12), 1819–1827 (2004)
  11. T. Lutas, V. Kostopoulos, Health monitoring of carbon/carbon, woven reinforced composites. Damage assessment by using advanced signal processing techniques. Part I: Acoustic emission monitoring and damage mechanisms evolution. *Compos. Sci. Technol.* **69**(2), 265–272 (2009)
  12. B.L. Yang, X.M. Zhuang, T.H. Zhang, X. Yan, Damage mode identification for the clustering analysis of AE signals in thermoplastic composites. *J. Nondestruct. Eval.* **28**(3–4), 163–168 (2009)
  13. D.G. Aggelis, N.M. Barkoula, T.E. Matikas, A.S. Paipetis, Acoustic structural health monitoring of composite materials: damage identification and evaluation in cross ply laminates using acoustic emission and ultrasonics. *Compos. Sci. Technol.* **72**(10), 1127–1133 (2012)
  14. M.A. Hamstad, A review: acoustic emission, a tool for composite materials studies. *Exp. Mech.* **26**(1), 7–13 (1986)
  15. M. Fotouhi, F. Pashmforoush, M. Ahmadi, R.A. Oskouei, Monitoring the initiation and growth of delamination in composite materials using acoustic emission under quasi-static three-point bending test. *J. Reinf. Plast. Compos.* **30**(17), 1481–1493 (2011)
  16. A.R. Oskouei, M. Ahmadi, Acoustic Emission characteristics of mode I delamination in glass/polyester composites. *J. Compos. Mater.* **44**(7), 793–807 (2010)
  17. A.B. de Moraes, M.F. de Mourab, A.T. Marquesb, P.T. de Castro, Mode-I interlaminar fracture of carbon/epoxy cross-ply composites. *Compos. Sci. Technol.* **62**(5), 679–686 (2002)
  18. I. Silversides, A. Maslouhi, G. LaPlante, Acoustic emission monitoring of interlaminar delamination onset in carbon fibre composites. *Struct. Health. Monit.* **12**(2), 126–140 (2013)
  19. J.R. Reeder, J.H. Rews, Mixed-mode bending method for delamination testing. *AIAA J.* **28**(7), 1270–1276 (1990)
  20. A. Szekrenyes, J. Uj, Over-leg bending test for mixed-mode I/II interlaminar fracture in composite laminates. *Int. J. Damage Mech.* **16**(1), 5–33 (2007)
  21. M. Fotouhi, H. Heidary, M. Ahmadi, F. Pashmforoush, Characterization of composite materials damage under quasi-static three-point bending test using wavelet and fuzzy C-means clustering. *J. Compos. Mater.* **46**(15), 1795–1808 (2012)
  22. J. Bohse, Acoustic emission characteristics of micro-failure processes in polymer blends and composites. *Compos. Sci. Technol.* **60**(8), 1213–1226 (2000)
  23. M. Salavatian, L.V. Smith, The effect of transverse damage on the shear response of fiber reinforced laminates. *Compos. Sci. Technol.* **95**, 44–49 (2014)
  24. K.W. Campbell, P.H. Mott, Damage tolerance in glass reinforced polymer laminates. *Compos. Sci. Technol.* **95**, 21–28 (2014)
  25. F. Ciampa, M. Meo, A new algorithm for acoustic emission localization and flexural group velocity determination in anisotropic structures. *Composites A* **41**(12), 1777–1786 (2010)
  26. R. Hill, R. Brooks, D. Kaloedes, Characterization of transverse failure in composites using acoustic emission. *Ultrasonics* **36**(1), 517–523 (1998)
  27. J.J. Scholey, D.W. Paul, R.W. Michael, I.F. Michael, Quantitative experimental measurements of matrix cracking and delamination using acoustic emission. *Compos. Part A* **41**(5), 612–623 (2010)
  28. R. Gutkin, C.J. Green, S. Vangrattanachai, S.T. Pinho, P. Robinson, P.T. Curtis, On acoustic emission for failure investigation in CFRP: pattern recognition and peak frequency analyses. *Mech. Syst. Signal Process.* **25**(4), 1393–1407 (2011)
  29. T. Czigány, Special manufacturing and characteristics of basalt fiber reinforced hybrid polypropylene composites: mechanical properties and acoustic emission study. *Compos. Sci. Technol.* **66**(16), 3210–3220 (2006)
  30. N. Ativitavas, T. Pothisiri, T.J. Fowler, Identification of fiber-reinforced plastic failure mechanisms from acoustic emission data using neural networks. *J. Compos. Mater.* **40**(3), 193–226 (2005)
  31. N. Godin, S. Hugueta, R. Gaertner, L. Salmon, Clustering of acoustic emission signals collected during tensile tests on unidirectional glass/polyester composite using supervised and unsupervised classifiers. *NDT & E Int.* **37**(4), 253–264 (2004)
  32. T.P. Philippidis, V.N. Nikolaidis, A.A. Anastassopoulos, Damage characterization of carbon/carbon laminates using neural network techniques on AE signals. *NDT & E Int.* **31**(5), 329–340 (1998)
  33. R. de Oliveira, A.T. Marques, Health monitoring of FRP using acoustic emission and artificial neural networks. *Comput. Struct.* **86**(3–5), 367–373 (2008)
  34. P.F. Liu, J.K. Chu, Y.L. Liu, J.Y. Zheng, A study on the failure mechanisms of carbon fiber/epoxy composite laminates using acoustic emission. *Mater. Des.* **37**, 228–235 (2012)
  35. Chinese National Standard, *Fiber-reinforced Plastic Composites—Determination of Flexural Properties* (Chinese National Standardization Management Committee, Beijing, 2005) (In Chinese)
  36. Chinese Aerospace Industry Corporation, *Chinese Spaceflight Industry Standard Acoustic Emission Inspection Method of Composite Structure* (Number QJ2914-97). Beijing: Chinese Aerospace Industry Corporation (1997) (In Chinese)
  37. G.M. Liu, *Nondestructive Inspection Technology* (National Defence Industry Press, Beijing, 2006) (In Chinese)
  38. X.J.N. Fang, Z.Q. Zhou, B.N. Cox, Q.D. Yang, High-fidelity simulations of multiple fracture processes in a laminated composite in tension. *J. Mech. Phys. Solids* **59**(7), 1355–1373 (2011)
  39. J.H. Williams, S.S. Lee, Acoustic emission monitoring of fiber composite materials and structures. *J. Compos. Mater.* **12**(4), 348–370 (1978)